FED-Vol. 137, Advances in Finite Element
Analysis in Fluid Dynamics
ASME 1992

C4

# NUMERICAL ANALYSIS OF 3-D ARTERIAL FLOWS IN DOUBLE CURVED FEMORAL ARTERY OF MAN

**Rupak K. Banerjee and Young I. Cho**
Department of Mechanical Engineering and Mechanics
Drexel University
Philadelphia, Pennsylvania

**Lloyd H. Back**
Jet Propulsion Laboratory
California Institute of Technology
Pasadena, California

## ABSTRACT

A three-dimensional steady flow simulation at $Re_{peak}$=580 was made in a smooth reverse curvature model that conformed to the gentle "S" shape from a human left femoral artery angiogram. The objective of this numerical investigation was to find the changes in velocity profile, shear stress, and pressure drop occurring in the double-curved arterial vessel. At the outer wall in the first bend region, where blood impinges, the wall shear stress approached 40 dyne/cm$^2$ - a value nearly twice as large as in the straight upstream segment. Conversely, at the inner wall in the first bend, a low shear stress region was found where the value of the shear stress was consistently smaller than that in the straight section. The initiation of centrifugal effects caused by the first bend could be clearly seen but, due to close proximity of the reverse curvature the double-spiraling motion was not observed. Further, the strong momentum effect due to reverse curvature overshadowed the centrifugal effect of first bend. Hence, only near the end of the second bend did the centrifugal effect due to the second bend result in a double-spiraling motion. In addition, the numerically calculated pressure drop data were in agreement with prior experimental values.

## NOMENCLATURE

| | | |
|---|---|---|
| d | = | lumen diameter (cm) |
| p | = | pressure |
| Q | = | volume flow rate (cm$^3$/min) |
| r | = | radial distance in lumen or normal to streamline (cm) |
| $r_c$ | = | radius of curvature of curved segment (cm) |
| $r_w$ | = | lumen radius (cm) |
| Re | = | Reynolds number based on lumen diameter $(4Q)/(\pi\nu d)$ |
| z | = | axial distance along curved model (cm) |
| y | = | distance along radius of curvature (cm) |
| x | = | distance perpendicular to radius of curvature (cm) |
| w | = | axial velocity in direction z (cm/sec) |
| v | = | transverse velocity in direction y (cm/sec) |
| u | = | transverse velocity in direction x (cm/sec) |
| $\theta$ | = | angular distance from curved inlet |
| $\kappa$ | = | Dean number, Re $(r_w/r_c)^{1/2}$ |
| $\mu$ | = | viscosity (poise) |
| $\nu$ | = | kinematic viscosity $(=\mu/\rho)$ |
| $\rho$ | = | density |
| $\tau_w$ | = | wall shear stress |
| $\phi$ | = | circumferential angle measured from the outer curvature |

Subscripts

| | | |
|---|---|---|
| 1 | = | in the first bend |
| 2 | = | in the second bend |

## INTRODUCTION

Some segments of the femoral artery of humans contain a distal curve in the opposite direction in addition to the single curvature, forming a gentle "S" shape. The current numerical investigation was performed to predict and identify the complex flow pattern generated in the "S" shaped model. Of specific interest here is the effect of arterial curvature reversal on the shear stress and fluid particle motion near the wall and the relative change in the overall flow behavior in reverse curvature regions compared to a straight lumen. The femoral artery is useful in isolating the effect of vessel curvature on hemodynamics and atherosclerotic lesion formation and growth because it has relatively few branches below the major profunda femoris branch and relatively gradual curvature with small angular changes. The "S" shape geometry, identical to the flow model used by Back et al. (1988) for their flow visualization study, was chosen because experimental data for Newtonian fluids (i.e., 33% sugar-water solution) is available from the previous work. The literature review illustrated in their experimental work has not been repeated here.

Berger et al. (1983) have reviewed flow in single curved pipes, including entrance region, which indicates the complexity of fluid dynamics in regions where the radius of curvature is constant along the pipe. Solving the full-elliptic Navier-Stokes equations, Soh and Berger (1984) studied laminar entrance flow in a curved pipe. They have identified that separation and the magnitude of the secondary flow are found to be greatly influenced by the curvature ratio. With reverse curvature, the flow field is even more complex. Ghia et al. (1987) numerically studied a fully developed incompressible flow in a square and polar cross-section curved duct for a Dean number up to 900 which corresponds to a Reynolds number of approximately 9,000. Detailed velocity measurements for a 90 degree bend for a circular cross section tube have been reported by Bovendeerd et al. (1987). Laser- Doppler velocity measurements were obtained for a curvature ratio $r_w/r_c$ of 1/6, Reynolds number 700 and Dean number 286.

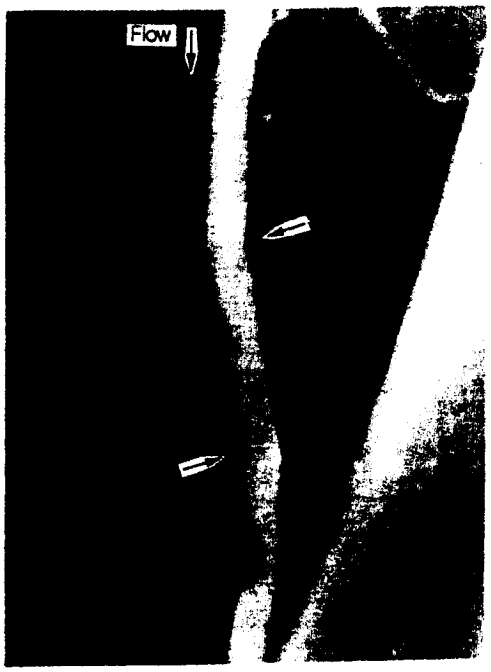


Fig. 1 Reverse curvature portion of a femoral artery angiogram of a patient. Blood flow is from top to bottom . The inner curvatures curvatures have far more lesions than the outer curvatures even though the curvature reverses.

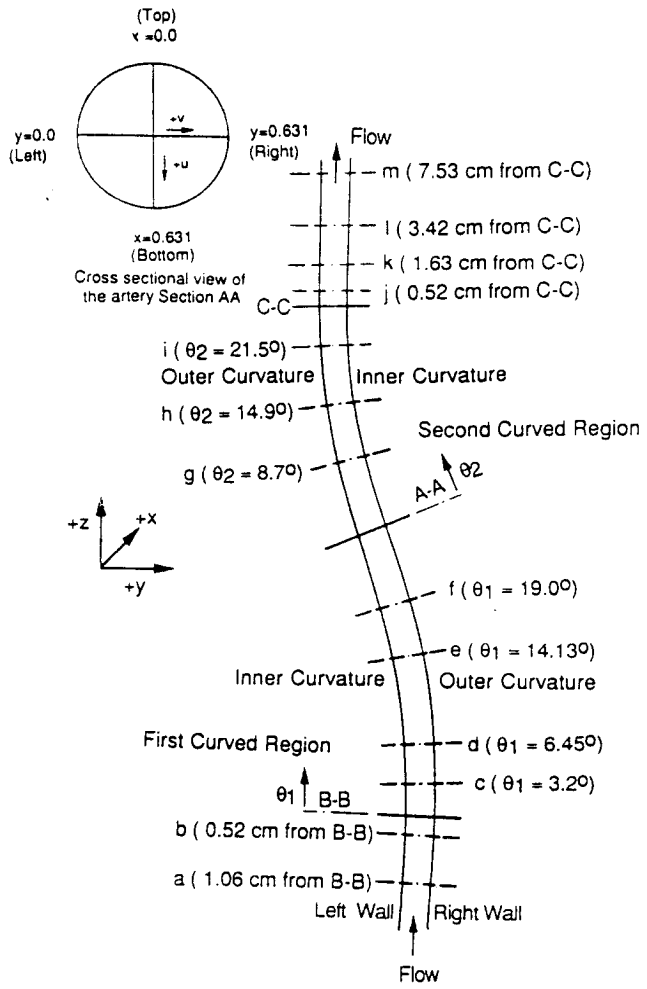


Fig. 2 Analyzed reverse curvature geometry showing outer and inner wall. a to m indicates the plane of observed velocity profiles.

## FLOW GEOMETRY

Figure 1 shows an angiogram of a portion of a "S" shaped human femoral artery (Back et al. (1988)). This proximal vessel segment bends with an almost constant radius of curvature $r_{c1}$ = 14 cm, and the distal segment bends in the opposite direction with a radius of curvature $r_{c2}$ = 12 cm in Hunter's canal where there is also some curvature normal to the plane of the angiogram. The length of the double (reverse) curvature vessel shown is about 13 cm and the vessel diameter is 6 ~ 7 mm. The segment which is distal to the profunda femoris branch has some relatively small branches, and there is negligible vessel taper. In this case the inner curvatures have far more lesions, as evident by the X-ray shadow (Fig. 1), than the outer curvatures, even though the curvature reverses.

A three-dimensional mesh of the reverse curvature shown in Fig. 2 was made to conform to the size and "S" shape of the human left femoral artery angiogram. The inside diameter of the model is 0.631 cm, and the radii of the first and second curvatures are $r_{c1}$ = 14.5 cm and $r_{c2}$ = 11.6 cm, where the subscript 1 denotes the value in the first curved region and the subscript 2 the value in the second curved region. The subtended angles of the first and second curved regions are $\theta_1$ = 26.5 deg. and $\theta_2$ = 26.5 deg. The corresponding ratios of the model radius to radius of curvature are $r_w/r_{c1}$ = 0.0218 and $r_w/r_{c2}$ = 0.0272.

In the current study, a physiological range of peak Reynolds number of 580 for resting mean femoral artery flow rate in man (Patel et al. (1965)) was investigated. The viscosity and density are 0.04 poise and 1.05 gm/cm$^3$. For flow simulation it is reasonable to incorporate the infinite shear rate viscosity of 0.04 poise for the peak Reynolds number case. The Dean number is defined as

$$\kappa = Re\left[\frac{r_w}{r_c}\right]^{1/2} = \left[\frac{4}{\pi}\frac{Q}{vd}\right]\left[\frac{r_w}{r_c}\right]^{1/2} \qquad (1)$$

and the respective Dean numbers for the first and second bends are $\kappa_1$ = 85.1 and $\kappa_2$ = 95.2 where Q= volume flow rate (cm$^3$/min) and v=

Table 1.
Comparison of Curved Geometry.

| Investigator | Type of Investigation | $r_w/r_c$ | Reynolds No. | Dean No. | Inlet Vel. Profile |
|---|---|---|---|---|---|
| Soh & Berger+ | Theoretical | 1/7 & 1/20 | 480-3000 | 108-680 | Relatively Flat |
| Bovendeerd+ et al. | Experimental | 1/6 | 700 | 286 | Parabolic |
| Shirayama & Kuwahara+ | Theoretical | 1/7 | 484 | 183 | Uniform |
| Present Study* | Theoretical | 2/100-3/100 | 192 580 | 28-95 | Parabolic |

\+ Single Bend (non-physiological, i.e. in reference to the aortic arch configuration,but without the major branch arteries);
* Double Curvature (physiological);

kinematic viscosity ($=\eta/\rho$). It is observed that the $r_w/r_c$ studied here are very small- approximately 10 times less in magnitude than various reported values which are shown in Table 1. The use of the Dean number to characterize the flow is only descriptive since the flow field for vessels with curvature reversal depends on both Reynolds number and $r_w/r_c$ ratios.

## METHODS

This study deals with the time-independent solution of an incompressible, non-Newtonian fluid for the selected geometry (Fig. 2). The flow is defined by a rigid wall in a 3-dimensional domain. The flow of such a fluid is described by the conservation equations of mass and momentum. A finite element technique is used to solve the two conservation equations to obtain the velocity, pressure and wall shear stress distributions.

$$u_{i,i} = 0 \tag{2}$$

$$\rho(u_j u_{i,j}) = -p_{,j} + \mu[(u_{i,j} + u_{j,i})_{,j}] + \rho f_i \tag{3}$$

where $u_i$ is the ith component of the velocity vector, and P is the pressure, and the viscosity $\eta$. The present study has been conducted using a Cartesian coordinate system with the center of reference axis being located at the center of the tube inlet. In comparison to this, the Berger et al. (1983) study for a single bend was done in a Toroidal coordinate system where the reference axis was located not at the center of the tube but at a distance equivalent to the radius of the curvature. The Galerkin formulation using eight nodal brick elements is applied to discretize the above continuity and momentum equations, which results in a set of nonlinear algebraic equations of the form

$$K(v)\, v = F \tag{4}$$

where $K(v)$ is the global system matrix developed from the momentum balance, $v$ is the velocity unknowns, and F is the forcing function (including body forces and boundary conditions). Penalty formulation is used to solve the momentum equation. Often the FEM is not directly applied to the system of equations but rather to a perturbed system of equations in which the continuity requirement is weakened by:

$$u_{i,i} = -\varepsilon p \qquad \text{where } \varepsilon = 1 \times 10^{-6} \tag{5}$$

For a high aspect ratios of the elements, a small penalty parameter is recommended. Physically, this can be equated to simulating the flow having insignificant compressibility effect. This approach has the advantage of eliminating one of the dependent variable $p^*$, which is then recovered by post-processing from the velocity field by:

$$p^* = -u_i^*{}_{,i} / \varepsilon \tag{6}$$

The matrix equation, representing a discrete analog of the original equations for an individual fluid element, is constructed and solved using the most conservative successive substitution method. In general, the convergence was achieved after the eighth iteration. Considering the long physiological entry length of the femoral artery, a fully developed flow was used as an inlet flow condition. No boundary condition was specified at the outlet. The finite-element computer code FIDAP is used to formulate and solve this matrix equation. The IBM-3090 is used together with TEMPLATE graphics for post-processing, and the results are down-loaded to an Apple-Macintosh II computer.

For validation of our numerical computation, three separate computer modeling with different convergence criteria (Table 2) are formed which are as follows: the relative velocity error with pect to previous step and relative error in the residue compared to ne initial value are set to be 2% and 1% respectively.

Table 2.
Numerical Accuracy Table for Re =580.

| Run No. | Velocity Convergence Tolerance | Residue Convergence Tolerance | Shear Stress* (dyne/cm$^2$) | CPU Time+ (min.) |
|---|---|---|---|---|
| 1. | 0.02 | 0.02 | 17.53 | 335 |
| 2. | 0.01 | 0.01 | 17.57 | 467 |
| 3. | 0.005 | 0.005 | 17.59 | 589 |

* Average shear stress has been obtained for the inlet of the straight section of the tube for both the right and left wall.
\+ For IBM-3090 Computer.

Furthermore, the overall convergence is confirmed by increasing the total number of meshes by 20% from that of the previous run, and the two results are compared to check for accuracy. When the improvement with 20% more meshes is less than one percent in velocity vectors and wall shear stress, the computation is considered accurate. This verification is particularly important since the wall shear stress and pressure values can be sensitive to the mesh size near the wall. 10,032 elements were used for mesh generation. The analysis of results is performed with the one with the least CPU time.

## RESULTS AND DISCUSSION

### *VELOCITY PROFILES*

Fluid motions in the reverse curvature femoral model are extremely complex since all three velocity components vary along the axial, radial, and circumferential directions. Figures 3 and 4 show axial (w: along z-direction) and transverse velocity (v: in the plane of curvature, along which centrifugal effects act), respectively. Transverse velocities v is presented along the x and y (inset in Fig. 2). In terms of relative magnitude, the variation in the transverse v-component is approximately 20~25% of the axial velocity component whereas it is 1-2% for the u-component (normal to the plane of curvature and axial direction). The u-component is not reported here.

Figure 3 shows axial velocities calculated at Re=580. Figures 3A and 3B present the data along the x direction in the first and second bends, respectively, and figures 3C and 3D shows the data along the y axis. A highly disturbed axial velocity profile is obtained as fluid encounters either of the 'S' shape bends. The axial velocity along the x axis is symmetric in the first bend region as demonstrated in Fig. 3A. The reduction of the axial core velocity with respect to the inlet velocity along the x direction is significant as the fluid advances (curves a ~ f) in the first bend. The axial velocity shown by curve f in Fig. 3A shows a significant dip at the center of the bend. Leaving the second bend region the axial velocity component gradually recovers (arrow in Fig. 3B) to the inlet Poiseuille flow value.

Figure 3C depicts the axial velocity along the y direction at various locations in the first bend. It is apparent from this figure that the axial flow is asymmetric in the plane of the curvature of the bend. The centrifugal effect due to the first bend is significant enough to shift the axial velocity to the outer wall, a phenomenon which can be seen by curve f in Fig. 3C, thus reducing the core axial velocity. Along the plane of symmetry the doubly peaked axial velocity profiles, as observed in the current study, are due to the centrifugal force which ultimately causes a secondary-flow vortex to occur.

As the fluid enters the second bend, the axial velocity begins to shift to the left (to the outer wall of the second bend) as seen from curves g ~ j in Fig. 3D. Further down the straight section, the axial velocity shifts back toward the right, as seen from curves j ~ m. It explains the increase in the core axial velocity shown in Fig. 3B (curves g ~ i) and quantify subsequent decreases (curves i ~ k). The curve k represents the case in which the axial velocity is skewed to the far left due to the centrifugal effect shown in Fig. 3D. The core axial velocity begins to increase again (curves k ~ m, Fig. 3B) as the axial velocity shifts back from the far left to the middle position

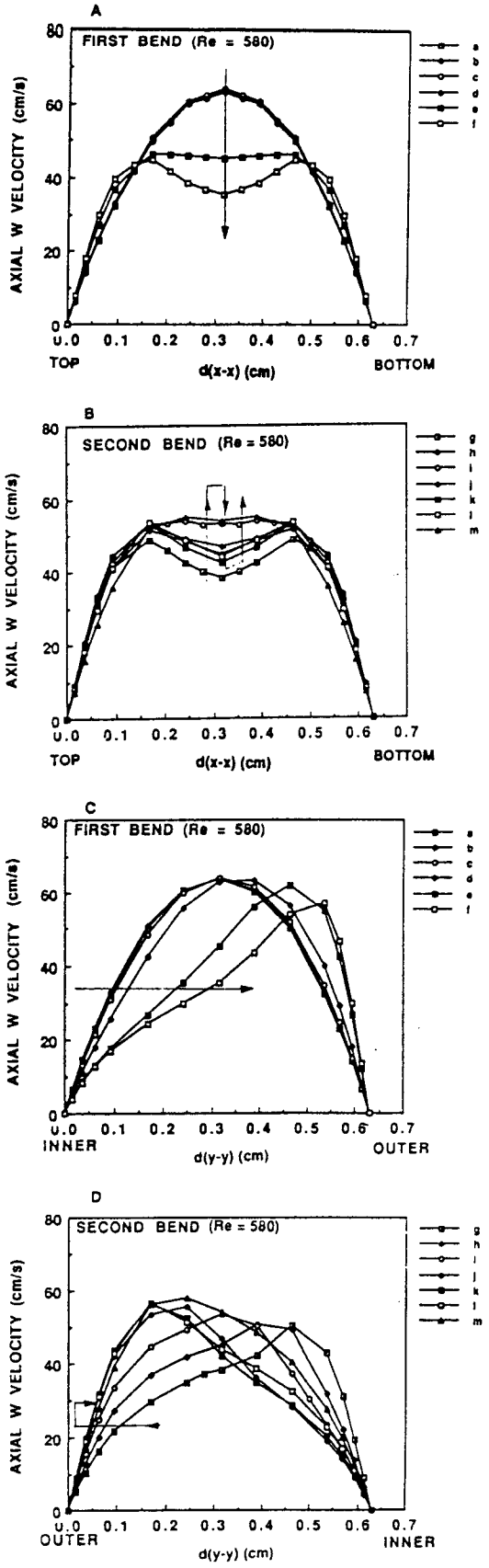


Fig. 3 Axial (w-component) velocity profile along x and y axis for Re = 580.

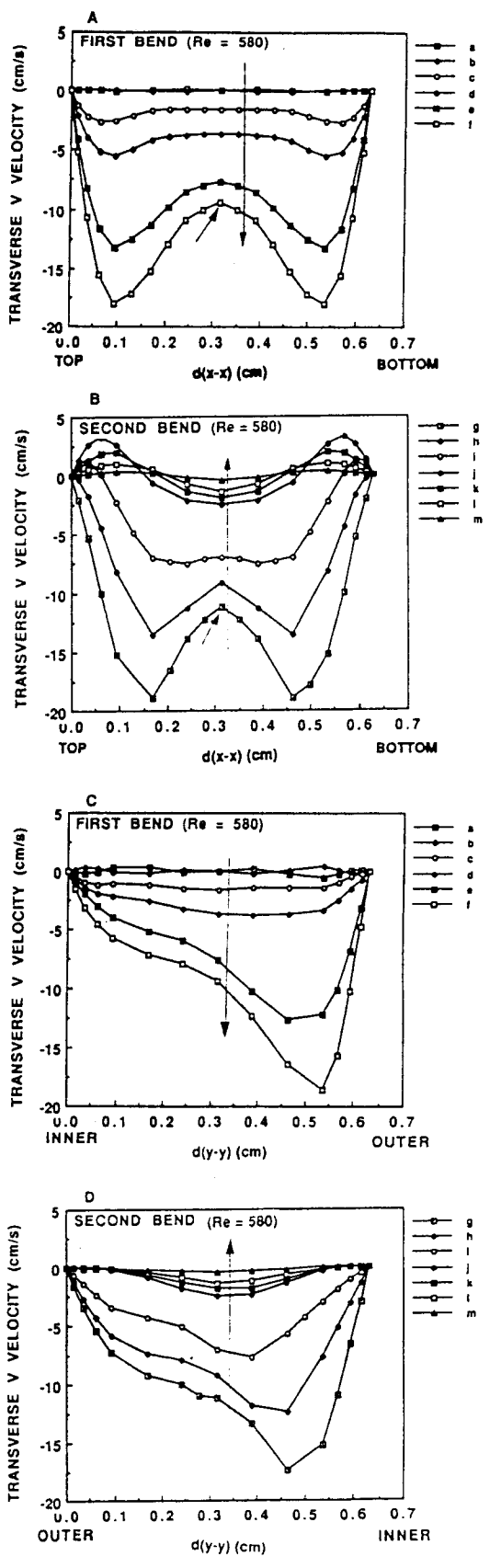


Fig. 4 Transverse (v-component) velocity profile along x and y axis for Re = 580.

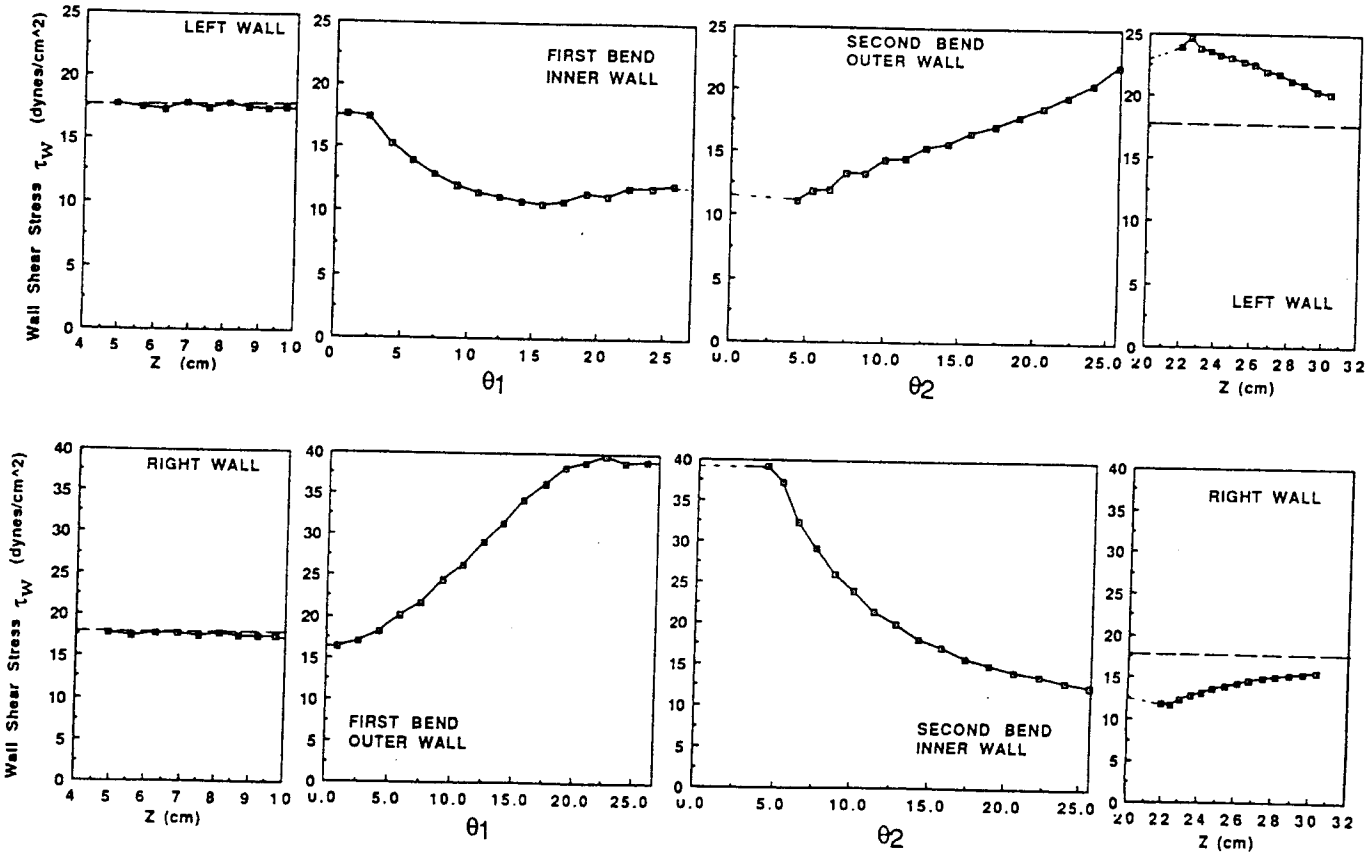


Fig. 5 Shear stress along left wall (top fig.) and right wall (bottom fig.) for Re = 580.

(curves k ~ m, Fig. 3D).

Figures 4A~4D present the transverse v-component of velocity along the x and y axis in both the first and second bend regions. Figure 4A shows the symmetric behavior of the transverse velocity along the x direction in the first bend region. The v-component is negative as the flow enters the first bend, and it gradually becomes more negative as the flow advances in the first bend.

This phenomenon can be categorized as an "early" bend effect whereas double-spiraling, centrifugal effect is a "late" bend effect. The centrifugal effect of the first bend is not large enough to produce a positive value for the v-component, which would have indicated the existence of the double-spiraling vortex. The fact that the v-component is negative indicates that fluid particles entering the first bend are pushed towards the inner wall of the first bend, rendering the negative value of v-component. A significant rise of the velocity at the center of each curve (arrows in Fig. 4A) signifies that the fluid particles near the center begin to feel the centrifugal effect due to the curvature in the first bend and attempt to move from the inner to the outer wall. Double spiral secondary motion due to the centrifugal effect in the first bend never occurs, as the fluid meets the second bend before the formation of a double spiral vortex structure.

Figure 4C presents the transverse velocity along the y direction in the first bend region. As fluid particles enter the first bend the fluid particles near the outer wall are the first ones being pushed to the inner wall, while those at the core experiences less obstruction. Therefore the maximum velocity of the transverse v-component occurs not at the center but near the outer wall in the first bend. This finding suggests that throughout the first bend the centrifugal effect (i.e., pushing fluid to the outer wall) is much smaller than the force caused by the outer wall (i.e., pushing fluid to the inner wall). The magnitude of the maximum v-component velocity increases as fluid moves into the first bend. In order to maintain mass conservation, the increase in the v-component velocity is accompanied by a corresponding decrease in the w-component velocity in the first bend, as seen earlier in Figs. 3A and 3C.

In Fig. 4D the transverse velocities are shown at various locations of the second bend. As the fluid enters the second bend, the decrease in the magnitude of the negative v-component indicates that the fluid is being pushed from the outer to the inner wall - a momentum effect of the second bend. Subsequently, as the fluid reaches the later part of the second bend, a dominant centrifugal effect due to the second bend is observed. A positive transverse velocity in the vicinity of the wall, while the fluid maintains negative velocities elsewhere (curves i ~ l, Fig. 4B), indicates of a double spiral secondary motion. The inertia effect is balanced by the centrifugal effect at about $\theta_2$= 15~20 degrees. The magnitude of the double spiral secondary motion is more intense, and its inception is earlier as the Reynolds number increases.

## *SHEAR STRESS*

To help understand the overall flow behavior in the reverse curvature arterial model, the wall shear stress data is presented in Fig. 5. The top half of figure shows the wall shear stress data from the left wall in the plane of the curvature, which includes the inner wall in the first bend and the outer wall in the second bend. The bottom half presents the wall shear stress profile from the right wall, which includes the outer wall in the first bend and the inner wall in the second bend. The wall shear stress calculated in the straight segment prior to entering the first bend, shown in Table 2 for all the three different convergence criteria, indicated agreement within 0.4% with the analytical prediction (17.6 dyne/cm$^2$) based on Poiseuille flow given as dashed lines in Fig. 5, thus confirming the validity of the current numerical computation.

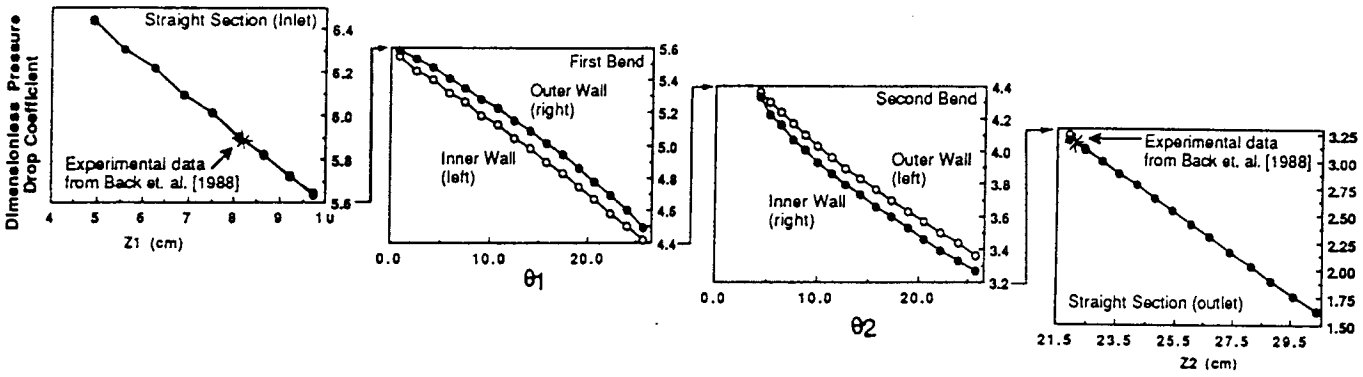


Fig. 6 The dimensionless pressure drop coefficient along the inner and outer wall of the model (Re=580).

As the fluid moves into the first bend, the wall shear stress gradually increases along the outer wall from the Poiseuille flow value of 17.5 dyne/cm$^2$ to a maximum value of 39.6 dyne/cm$^2$ at the end of the first bend. On the other hand, the shear stress decreases along the inner wall from 17.5 dyne/cm$^2$ to a plateau value of 11.5 dyne/cm$^2$ at $\theta_1 = 10^o$ and remains unchanged until the fluid enters the second bend. The data from the first bend region clearly indicates that the outer wall in the first bend region experiences a much larger shear stress than the inner one, which may be attributed to flow impingement associated with the outer wall of the first bend. The shear stress along the inner wall is substantially smaller than the value predicted by Poiseuille flow.

As the fluid moves into the second bend, the shear stress along the outer wall (i.e., left wall) gradually increases, reaching a value of 21.9 dyne/cm$^2$ at the end of the second bend. The first set of data in the second bend is located at $\theta_2$=4.3°. Hence, a dashed line was used to connect the last data point in the first bend and the first data point in the second bend in Fig. 5. As the fluid continues to move into the left side of the straight section, the shear stress continues to increase to a maximum value of 24.7 dyne/cm$^2$ before it begins to gradually decrease to the Poiseuille flow value shown as a dashed line. This increase may be attributed to the fact that fluid particles entering into the straight section experience the reverse curvature thus increasing the wall shear stress locally. In this region the magnitude of the wall shear stress is much smaller than that of the first bend. Along the y-axis it is observed that the magnitude of the axial velocity gradient (Figs. 3C and 3D), a measure of shear stress, is smaller at the outer wall of the second bend than at the outer wall of the first bend. Therefore, the wall shear stress is considerably less near the proximity of the second bend. Along the inner wall in the second bend the wall shear stress decreases, resembling an exponential profile to a minimum value of 12 dyne/cm$^2$ and then begins to recover as the fluid enters the straight section.

*PRESSURE DROP*

The dimensionless pressure drop coefficient along the double curved vessel in the plane of the curvature was calculated and is shown in Fig. 6. The pressures in the two straight sections (i.e., before the first bend and after the second bend) are found to decrease linearly as predicted. The overall pressure drop across the double curved vessel, when compared with the experimental data reported earlier by Back et al. (1988), shows agreement. Non-dimensional pressure drop between the outlet and inlet of the double curvature has been experimentally determined to be 2.63 (x- marks in Fig. 6) whereas a value of 2.52 has been obtained numerically. A deviation of less than 7% has been observed. Additionally, in this investigation, the detailed pressure drop along the outer and inner curvature have been reported.

In the double curved section, interesting results of local pressure changes have been observed. In the first bend, the pressure on the outer wall (right wall) is larger than on the inner wall (left wall). In the second bend, the pressure on the outer wall (left wall) is also larger than on the inner wall (right wall). When a flow in a curved tube is fully developed, the pressure at the inner wall is higher than that at the outer wall, resulting in the double-spiral vortex, the centrifugal effect. For a developing flow in a single curved tube the outer wall experiences higher pressure in comparison to the inner one, clearly suggesting that for the developing flow region, as we have in the double curved vessel, the pressure at the outer wall is greater than at the inner wall both in the first and second bends.

## SUMMARY AND CONCLUSIONS

In spite of the inherent difficulties associated with the presentation of 3-D flow field data, the current study attempted to show detailed axial and transverse velocity profiles at various locations in the first and second bends, in addition to showing the wall shear stress and pressure distributions along the inner and outer walls in the plane of the curvature. The highlights of the current numerical study are summarized as follows:

1. The double-spiral-secondary motion, governed by the Reynolds number, the lumen diameter, and the radius of curvature of the vessel, does not occur in this "S" shape arterial model until the fluid reaches the end of the second bend. The numerical investigation of secondary flow for the early region of first bend was found to be directed completely towards the inner curvature. This phenomenon can be categorized as an "early" bend effect whereas double-spiraling is a "late" bend effect. Separation and the magnitude of the secondary flow have been found by others to be greatly influenced by the curvature ratio. In this investigation, due to the very mild curvature ratios for the first and second bends, the inertia or the impingement effects dominate the centrifugal effects.

2. The highest wall shear stress occurs at the outer wall of the first bend, being 40 dyne/cm$^2$, which is much greater than the corresponding Poiseuille flow value of 17.5 dyne/cm$^2$. Another higher shear stress region is generated at the outer wall of the straight section right after the second bend, 25 dyne/cm$^2$. In contrast, the shear stress decreases along the inner wall of the first bend from 17.5 dyne/cm$^2$ to a plateau value of 11.5 dyne/cm$^2$ and remains unchanged until the fluid enters the second bend. Along the inner wall of the second bend, the wall shear stress decreases exponentially almost to a minimum value of 12 dyne/cm$^2$ at the end of the second bend and begins to recover as the fluid enters the straight section.

3. A higher shear stress region, obtained in the present investigation, helps in scavenging the cell walls of deposits and in increasing mass transfer of gaseous species such as oxygen. However, not much is known about the potential trauma to endothelial cells associated with moderately elevated shear stress. Conversely, a lower shear stress region found in the inner wall does not have this cleansing mechanism and may cause reduction in the mass transfer of oxygen [Back et al. 1977, Nerem and Levesque 1987] and therefore susceptible to the deposition of macromolecules, e.g. cholesterol, lipoproteins and other lipid derivatives [Caro et al. 1969, Nerem and Levesque 1987], leading to the development of atherosclerosis.

4. The pressure at the outer wall of the first and second bends is greater than that at the inner wall, a phenomenon similar to that of a developing flow in a curved tube.

Though this study is limited and does not explore the flow phenomenon for an entire cardiac pulse, the flow simulation for the peak flow may be considered adequate to represent the complicated 3-D motion in the double bend with reverse curvature geometry- a site which is prone to develop lesions. An analysis for a full cardiac cycle may definitely show variation of flow parameters with time, but the overall trend of flow remains unaltered. Detailed 3-D study, presented here, may be useful in the future for an in-depth analysis of flow for a complete pulse cycle.

## REFERENCES


Back, L. H., Back, M.R., Kwack,E.Y. and Crawford, D. W. (1988) Flow measurements in a human femoral artery model with reverse lumen curvature. *ASME J. Biomech. Engrg.* **110**, 300-309.

Back, L. H., Radbill, J.R. and Crawford, D. W. (1977) Analysis of oxygen transport from pulsatile, viscous blood flow to diseased coronary arteries of man. *J. Biomech.* **10**, No 11/12, 763-774.

Berger, S. A., Talbot, L., and Yao, L. S. (1983) Flow in Curved Pipes. *Ann. Rev. Fluid Mech.* **15**, 461-512.

Bovendeerd, P. H. M., Van-Steenhoven, A. A., Van-De-Vosse, F. N., Vossers, G., (1987) Steady entry flow in a curved pipe. *J. Fluid Mech.* **177**, 233-246.

Caro, C. G., Fitz-Gerald, J. M. and Schroter, R. C. (1969) Arterial wall shear and distribution of early atheroma in man. *Nature Lond.* **223**, 1159-1161.

FIDAP Manual, (1991), Fluid Dynamics International, Inc., Evanston, Illinois

Ghia, K. N., Ghia,U., Shin,C.T. (1987) Study of fully developed incompressible flow in curved ducts, using a multi-grid technique. *ASME J. Fluid Eng.* **109**, 226-236.

Narem, R. M. and Levesque, M. J. (1987) Fluid mechanics in atherosclerosis. *Handbook of Bioengineering* (R. Skalak and S. Chien Ed.) Chap. **21**, 21.1-21.22.

Patel, D. J., Greenfield, J. C., Jr., Austen, W. G., Morrow, A. G., and Fry, D. L. (1965) Pressure-Flow Relationships in The Ascending Aorta and Femoral Artery of Man. *Journal of Applied Physiology* **20**, 459-463.

Shirayama, S., Kuwahara, K. (1987) Computational study of flow in a curved pipe with circular cross section. *KSME Journal* **1**, No.1, 55-59.

Soh, W. Y., and Berger, S. A. (1984) Laminar Entrance Flow in a Curved Pipe. *J. Fluid Mech.* **148**, 109-135.